Journal of Biomolecular NMR, **17:** 295–304, 2000.
KLUWER/ESCOM

The auto-orientation in high magnetic fields of oxidized cytochrome b_{562} as source of constraints for solution structure determination

Fabio Arnesano[a], Lucia Banci[a], Ivano Bertini[a,*], Karin van der Wetering[a,**], Michael Czisch[b] & Robert Kaptein[b,*]

[a]*Magnetic Resonance Center, University of Florence, Via Luigi Sacconi 6, I-50019 Sesto Fiorentino, Italy;* [b]*Bijvoet Center for Biomolecular Research, University of Utrecht, Padualaan 8, 3584 CH Utrecht, The Netherlands*

Received 9 February 2000; Accepted 10 May 2000

Key words: cytochromes, magnetic susceptibility anisotropy, paramagnetism, residual dipolar couplings, solution structure

Abstract

^{15}N-^{1}H ^{1}J couplings were measured at 500 MHz and 800 MHz for ^{15}N enriched oxidized cytochrome b_{562} from *E. coli*. The magnetic field dependence of 70 ^{1}J values, which could be measured without signal overlap, shows that there is a molecular magnetic anisotropy which provides partial molecular orientation in the magnetic field and, consequently, residual dipolar couplings (rdc). The rdc were used as further constraints to improve the existing structure [Arnesano et al. (1999) *Biochemistry*, **38**, 8657–8670] with a protocol which uses the rhombic anisotropy [Banci et al. (1998) *J. Am. Chem. Soc.*, **120**, 12903–12909]. The overall large molecular magnetic anisotropy has been found to be determined by both the low spin iron (III) and the four helix bundle structure magnetic susceptibility anisotropy contributions.

Abbreviations: cyt b_{562}, cytochrome b_{562}; rdc, residual dipolar couplings; pcs, pseudocontact shifts; RMSD: root mean square deviation.

Introduction

Residual dipolar couplings (rdc hereafter), which result from partial orientation of the molecule in solution when located in high magnetic fields (Lohman and Maclean, 1978,a,b, 1981; Domaille, 1980; Bothner-By et al., 1981, 1984, 1985; Gayathri et al., 1982; van Zijl et al., 1984; Bothner-By, 1996), are a precious source of structural constraints (Tolman et al., 1995; Tjandra et al., 1996, 1997; Banci et al., 1998; Clore et al., 1998; Clore and Gronenborn, 1998; Bayer et al., 1999; Biekofsky et al., 1999; Bolon et al., 1999; Fischer et al., 1999). The partial orientation is caused by the molecular magnetic anisotropy which, in case of diamagnetic proteins, depends on the folding and the shape of the protein itself.

In the case of paramagnetic metalloproteins, with sizeable magnetic susceptibility anisotropy originating from the metal ion, a sizeable partial orientation is expected. Up to now, oxidized cytochrome b_5 has been investigated (Banci et al., 1998), where the contribution to the molecular magnetic anisotropy was mainly determined by the paramagnetic anisotropy of the metal ion itself. The latter was decreased by the diamagnetic contribution of the heme ring, whose axial anisotropy has opposite direction with respect to that of the metal ion.

The oxidized cytochrome b_{562} (cyt b_{562} hereafter) from *E. coli* contains a heme with an unpaired electron, like cyt b_5, and has a particular structure which is known as four-helix bundle. Its solution structure is already available (Arnesano et al., 1999). The iron ion cycles between the 3+ and 2+ oxidation states,

*To whom correspondence should be addressed. E-mail: bertini@cerm.unifi.it; kaptein@nmr.chem.uu.nl

**Present address: Institute of Chemistry, University of Leiden, Leiden, The Netherlands.

always in the low spin state. The iron ion is six coordinated to a *b*-type heme and to a histidine and a methionine as axial ligands. Helices constitute 80% of the total protein, the rest of the residues being involved in loops. We show that the protein undergoes significant residual orientation, which can be used as a source of structural constraints and, indeed, rdc's have been here introduced to refine the solution structure. Furthermore, the relative contributions to the overall magnetic anisotropy of the molecule have been addressed, i.e. (i) the diamagnetic protein contribution, which is determined by the particular protein structure, the typical four-helix bundle folding (Hamada et al., 1995), (ii) the paramagnetic contribution of the Fe^{3+} ion, which was previously determined through the analysis of pseudocontact shifts (pcs) and (iii) the diamagnetic contribution of the heme.

Materials and methods

Sample preparation

The ^{15}N labeled *Escherichia coli* cyt b_{562} was prepared as described before (Arnesano et al., 1999). The samples used for NMR spectroscopy are 3 mM in protein, in 500 mM phosphate buffer at pH 4.8 in 90% H_2O and 10% D_2O.

The reduced form of cyt b_{562} was obtained by adding 75 μL of a degassed 0.086 M solution of sodium dithionite to a degassed 2 mM sample of oxidized cyt b_{562}. Both solutions were in a 500 mM phosphate buffer at pH 4.8. Degassing was performed by putting the solutions under argon for at least 45 min. After reducing, the sample was kept under argon for another 15 min, after which the NMR tube was closed airtight.

NMR spectroscopy

NMR experiments were carried out at 25.0 °C on a Bruker AVANCE 800 operating at 800.13 MHz, and Bruker AVANCE 500 and VARIAN 500 spectrometers (the latter one was used for the oxidized form), operating at 500.13 MHz. The temperature was calibrated by measuring the difference in chemical shift between hydroxyl and methylene peaks of a sample of 80% ethyleneglycol in DMSO.

The intensities of cross peaks in a ^{15}N-^{1}H ^{1}J-modulated HSQC as a function of the 2Δ delay in the pulse sequence (I(2Δ)) are related to the experimental parameters and the N-H J couplings by the equation (Tjandra et al., 1996):

$$I(2\Delta) = I_0\,[-A + \cos(2\pi J_{NH}\Delta)]\exp\left(-\frac{2\Delta}{T_2^*}\right) \quad (1)$$

where I_0 is the intensity of the cross peak when Δ is null, *A* is a term which accounts for the unmodulated fraction of magnetization due to pulse imperfection and $1/T_2^*$ is the effective decay rate of the transverse ^{15}N magnetization. To account for the dephasing angle during the 180° ^{15}N pulse (Tjandra et al., 1996), the delay (2Δ in Equation 1) should be corrected by addition of a fraction $(2/\pi)$ of the refocusing 180° ^{15}N pulse duration.

As suggested (Tjandra et al., 1996), 2Δ values should be chosen as two sets of symmetric values around (2n+1)/2J, where n is an integer, in order to optimize the accuracy of the measurement of J. For this purpose three spectra were recorded with 2Δ delays of 47, 54 and 62 ms. The best values of n, that depend on the value of T_2^*, were found to be 4 and 5.

One set of 10 experiments at 800 MHz, each consisting of 48 scans for the oxidized and 16 scans for the reduced form, was performed with dephasing delays, 2Δ, of 45.2, 46.0, 47.6, 48.8, 50.2, 56.4, 57.8, 58.4, 60.0 and 61.0 ms and a control experiment was run with a dephasing delay of 45.2 ms. With the same 2Δ values two identical sets of 10 experiments, each consisting of 32 scans, were performed for both the oxidized and the reduced form at 500 MHz. In addition to the above 10 experiments, a further experiment was performed for the reduced protein at 500 MHz with a dephasing delay of 62.6 ms. The 180° ^{15}N pulse ranged from 60 to 70 μs on all three spectrometers.

After multiplication by a 90°-shifted sine-bell, the 2D spectra were baseline corrected. Cross peaks were integrated defining rectangular boxes at the noise level, except for overlapping cross peaks, for which smaller boxes were chosen in order to keep non-biased data. For the integration of the spectra that were recorded on the VARIAN 500 spectrometer, the NMRView program (Johnson and Blevins, 1994) was used. For the spectra that were recorded on the Bruker AVANCE 800 and AVANCE 500, the standard Bruker software was used.

Determination of the molecular magnetic susceptibility anisotropy

The Δrdc values are given by the difference of the $^{1}J_{NH}$ values measured at two different magnetic fields. To extract the dipolar coupling contribution, the Δrdc must be corrected for the contribution due to the

dynamic frequency shift (δ_{DFS}), which constitutes a non-negligible magnetic field-dependent contribution to apparent ^{1}H-^{15}N ^{1}J (Tjandra et al., 1996). Δrdc values are therefore given by the following relation:

$$\Delta\text{rdc} = -[(J_{800\ \text{MHz}} - J_{500\ \text{MHz}}) + (\delta_{\text{DFS }800\ \text{MHz}} - \delta_{\text{DFS }500\ \text{MHz}})] \quad (2)$$

The negative sign in Equation 2 takes into account that the ^{1}H-^{15}N ^{1}J is negative (Tolman et al., 1995).

δ_{DFS} values depend on the rotational regime of the molecule (Tjandra et al., 1996; Werbelow, 1996). In the case of axially symmetric rotational diffusion, the value of δ_{DFS} depends on the relative orientations of the diffusion and CSA tensors and on the orientation of the NH bond vector with respect to the two tensors (Tjandra et al., 1996; Werbelow, 1996). Each NH moiety will thus have a different value of δ_{DFS}. The equation for δ_{DFS} is:

$$\delta_{DFS}(B_0) = \frac{S^2}{40\pi^3} h(\sigma_\parallel - \sigma_\perp)\frac{\gamma_N\gamma_H}{r_{NH}^3} \left\{ \frac{(3\cos^2\eta_D - 1)(3\cos^2\eta_C - 1)}{1 + (\gamma_N B_0 \tau_1)^{-2}} + \frac{12\cos\eta_D\cos\eta_C\sin\eta_D\sin\eta_C\cos(\phi_D - \phi_C)}{1 + (\gamma_N B_0\tau_2)^{-2}} + \frac{3\sin^2\eta_D\sin^2\eta_C\cos(2\phi_D - 2\phi_C)}{1 + (\gamma_N B_0\tau_3)^{-2}} \right\} \quad (3)$$

where $\tau_1 = (6D_\perp)^{-1}$, $\tau_2 = (D_\parallel + 5D_\perp)^{-1}$, $\tau_3 = (4D_\parallel + 2D_\perp)^{-1}$. The angle between the ^{1}H-^{15}N vector and the unique axes of the diffusion tensor is η_D, and that between the axially symmetric CSA tensor and the diffusion tensor is η_C. The difference $\phi_D - \phi_C$ refers to the angle between projections of the unique axes of the dipolar and CSA tensors on the plane perpendicular to the unique axis of the diffusion tensor; h is Planck's constant, γ_N and γ_H are the gyromagnetic ratios for ^{15}N and ^{1}H, r_{NH} is the N-H internuclear distance (1.02 Å), B_0 is the external magnetic field and S^2 is the generalized order parameter.

Δrdc are given by the following equation (cf. van Zijl et al., 1984):

$$\Delta rdc = -\frac{1}{4\pi}\frac{\Delta B_0^2}{15kT}\frac{\gamma_H\gamma_N h}{4\pi^2 r_{HN}^3}\left[\Delta\chi_{ax}^{mol}(3\cos^2\theta - 1) + \frac{3}{2}\Delta\chi_{rh}^{mol}(\sin^2\theta\cos 2\phi)\right] \quad (4)$$

where $\Delta\chi_{ax}^{mol}$ and $\Delta\chi_{rh}^{mol}$ are, respectively, the axial and rhombic components of the molecular magnetic susceptibility anisotropy tensor, χ^{mol}, and θ and ϕ are polar coordinates describing the orientation of the N-H bond vector in the (axis) frame of the χ^{mol} tensor. The structural constraints, used in the present calculations, are the differences in rdc values (referred to as Δrdc) measured at two different fields (18.7 T and 11.7 T in this work).

The magnetic susceptibility tensor parameters are obtained by best fitting the experimental Δrdc values, corrected by the δ_{DFS}, to Equation 4 and by using as input the structural model calculated without their inclusion (Banci et al., 1998). The adjustable parameters are the $\Delta\chi_{ax}^{mol}$ and $\Delta\chi_{rh}^{mol}$ values, and the three independent direction cosines needed to define the orientation of the χ^{mol} tensor within the laboratory frame. When dealing with a family of conformers as obtained from solution structure calculations, a tensor for each member of the family can be obtained. Alternatively, all conformers are superimposed, by best fitting the coordinates of the backbone heavy atoms of the well-defined regions of the protein, and a single average χ^{mol} tensor is determined. In the fitting procedure, we followed the same approach already tested in the case of cytochrome b_5 (Banci et al., 1998), evaluating a single average tensor for the superimposed structure. In full analogy to the determination of the paramagnetic susceptibility tensor from pseudocontact shifts (Bertini et al., 1996; Banci et al., 1997; Bentrop et al., 1997; Arnesano et al., 1998, 1999), the minimized quantity is the square of the difference between calculated and experimental Δrdc values, introducing a tolerance of 0.1 Hz for the oxidized and 0.2 Hz for the reduced protein, which roughly corresponds to the mean value of the experimental error.

Introduction of residual dipolar coupling constraints in structure calculations

A routine implemented in PSEUDYANA has been used to include Δrdc constraints in the structure calculations of the oxidized form, as already done for cytochrome b_5 (Banci et al., 1998). The program needs only the $\Delta\chi_{ax}^{mol}$ and $\Delta\chi_{rh}^{mol}$ values as input parameters for the structure calculations, as the orientation of the χ^{mol} tensor in the molecular frame is adjusted by the program in order to minimize the target function. In addition to Δrdc, the structure of the oxidized form was calculated with 1653 non-redundant NOEs, 33 $^3J_{HNH\alpha}$ values and 357 pcs. The relative weights of all constraints were taken equal to 1 and the tolerance values T_i for Δrdc were equal to 0.1 Hz. The new family of conformers was used as input structural model to

Table 1. Parameters characterizing the χ_{ox}^{mol} and the χ_{red}^{mol} tensors of the oxidized and the reduced protein, respectively, and the χ_{ox}^{metal} tensor of cyt b_{562}

	χ_{red}^{mol} tensor[a,b]	χ_{ox}^{metal} tensor[a,c]	χ_{ox}^{mol} tensor[a,d]	Calculated χ_{ox}^{mol} tensor[e]
$\Delta\chi_{ax}$ ($/10^{-32}$ m^3)	1.6 ± 0.1	1.8 ± 0.2	-2.0 ± 0.4	-2.2 ± 0.3
$\Delta\chi_{rh}$ ($/10^{-32}$ m^3)	-0.4 ± 0.3	-0.4 ± 0.2	0.5 ± 0.3	0.7 ± 0.1
Deviation of the z axis from the normal to the heme plane (°)	88 ± 5	19 ± 7	98 ± 8	96 ± 9
Deviation of the y axis from the heme pyrrole Nβ-Nδ axis (°)	98 ± 15	25 ± 8	74 ± 15	58 ± 21

[a]The reported error on the $\Delta\chi$ parameters is the standard deviation from the mean of the 20 values obtained by fitting each conformer individually. The uncertainty on the angles was taken equal to the largest deviation from the optimal solution, yielding a sum of the squared differences between calculated and experimental Δrdc (or pcs) values smaller than twice the sum evaluated for the optimal solution itself.
[b]Obtained by fitting the 47 Δrdc's to Equation 4 using as input the refined PSEUDYANA family.
[c]Obtained from the fit of the 357 pseudocontact shifts to the refined PSEUDYANA family. The present values are calculated for comparison purposes, and are slightly different from those already reported, calculated on an energy-minimized family (Arnesano et al., 1999).
[d]Obtained by fitting the 70 Δrdc's to Equation 4 using as input the refined PSEUDYANA family.
[e]These parameters were obtained by summing the experimental χ_{red}^{mol} and the χ_{ox}^{metal} tensors.

re-estimate the tensor parameters, as described above, for a new refinement step. It is worth to remember that in the present system, the contribution to the residual dipolar coupling due to the rhombic anisotropy is not negligible, and thus we cannot assume an axially symmetric magnetic susceptibility anisotropy tensor (Tjandra et al., 1997; Banci et al., 1998).

Results and discussion

Determination of dipolar contribution to $^1J_{NH}$ values

The protein exists in solution as two species, in which the orientation of the heme group differs by a 180° rotation around the α-γ axis, in the ratio of 2:1 (Wu et al., 1991) and which are referred to as forms A and B, respectively. ^{1}H and ^{15}N assignments of the oxidized form had been previously performed (Arnesano et al., 1999) and the peaks were easily located in the maps. Only cross peaks arising from form A and cross peaks unresolved for both forms were used. Neglecting ^{15}N-^{1}H cross peaks which are degenerate, 70 ^{1}H-^{15}N ^{1}J couplings were measured at 800 and 500 MHz. Their values are available as Supplementary material, Table 1.

Peak volumes were fitted with the four parameters I_0, A, J_{NH} and T_2^* of Equation 1. The root-mean square difference between the results of the two sets of experiments recorded at 500 MHz was 0.06 Hz. This value is comparable to those previously reported for other systems (Tjandra et al., 1996; Tolman and Prestegard, 1996) and is an estimate of the random error. Furthermore, a systematic error between the experiments at 800 MHz and 500 MHz may also be present.

The orientation of the rotational diffusion tensor (D) in the protein frame is assumed to be similar to that of the inertia tensor (Tjandra et al., 1995). The relative values of the principal moments of the inertia tensor of oxidized cyt b_{562} can be calculated from structural data and are 1:0.96:0.37. The D tensor of cyt b_{562} is thus expected to be non-isotropic and essentially axially symmetric with a $D_\parallel/D_\perp$ ratio of 2.7. In the present case, by assuming an angle of 24° between the ^{1}H-^{15}N vector and the principal axis of the ^{15}N CSA tensor (Hiyama et al., 1988), a difference between parallel and orthogonal chemical shift for the CSA tensor of ^{15}N of −160 ppm, and a uniform S^2 value of 0.85, these differences were found to be at most 0.1 Hz. Thus, although the above parameters used to calculate the δ_{DFS} are only reasonable estimates rather than experimental values, only a minor error is introduced in the estimate of Δrdc. The observed values of ΔJ(800 MHz − 500 MHz) are plotted in Figure 1 and the resulting Δrdc are available as Supplementary material (Table 3).

Structure calculation results

Initial values for the $\Delta\chi^{mol}$ tensor parameters of cytochrome b_{562} were obtained by fitting the Δrdc values, using as input models the 20 conformers of the PSEUDYANA family previously obtained without Δrdc constraints (Arnesano et al., 1999). These

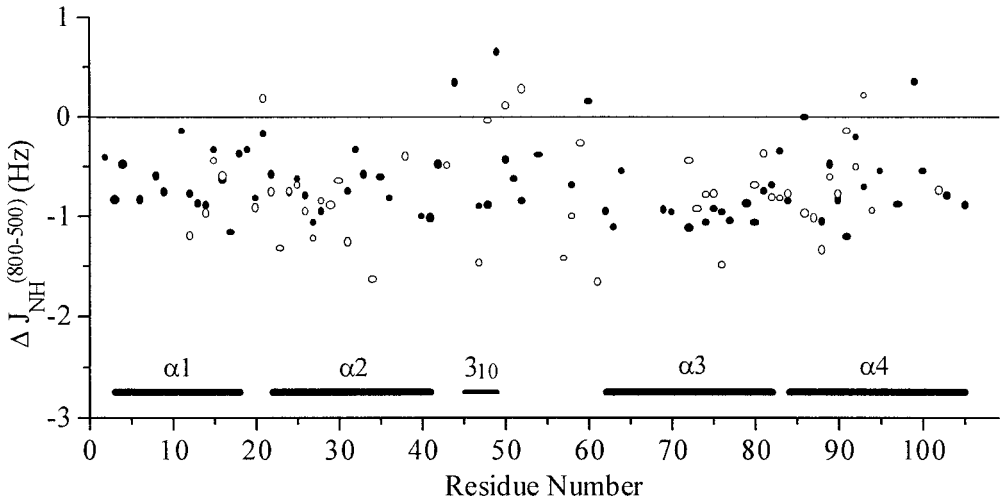

Figure 1. Experimental values of ΔJ_{NH} (800−500) per residue for the oxidized (solid circles) and reduced form (open circles). The bold lines at the bottom indicate the location of the α helices in the protein sequence. The thinner line indicates the location of the 3_{10} helix.

Table 2. Statistical analysis of structure calculations for oxidized cyt b_{562} run with NOE, pcs and $^3J_{HNH\alpha}$ only and with NOE, pcs, $^3J_{HNH\alpha}$ and Δrdc. All values are averaged over the best 20 conformers, unless otherwise indicated

	NOE, $^3J_{HNH\alpha}$, and pcs	NOE, $^3J_{HNH\alpha}$, pcs and Δrdc
Backbone RMSD[a] (residues 3–50 and 62–105) (Å)	0.42 ± 0.06	0.50 ± 0.10
NOE, $^3J_{HNH\alpha}$, pcs and van der Waals target function (Å^2)	0.76 ± 0.06	1.15 ± 0.11
Total target function (Å^2)	0.76 ± 0.06	1.34 ± 0.13
Average violation per NOE constraint (Å)	0.0054 ± 0.0003	0.012 ± 0.002
Average number of NOE violations > 0.2 Å per structure	0 ± 1	1 ± 1
Largest NOE violation (Å)[b]	0.31	0.46
Average violation per pcs constraint (ppm)	0.04 ± 0.01	0.04 ± 0.02
Average number of pcs violations > 0.5 ppm per structure	15 ± 2	16 ± 3
Largest pcs violation (ppm)[b]	0.9	1.1
Average violation per Δrdc constraint (Hz)	0.10 ± 0.06	0.03 ± 0.05
Average number of Δrdc violations > 0.1 Hz per structure	35 ± 3	20 ± 3
Largest Δrdc violation (Hz)[b]	1.3	0.6

[a]These values have been recalculated by using the present DYANA structures, as discussed in the experimental part, for comparison purposes.
[b]Largest violation among all 20 conformers.

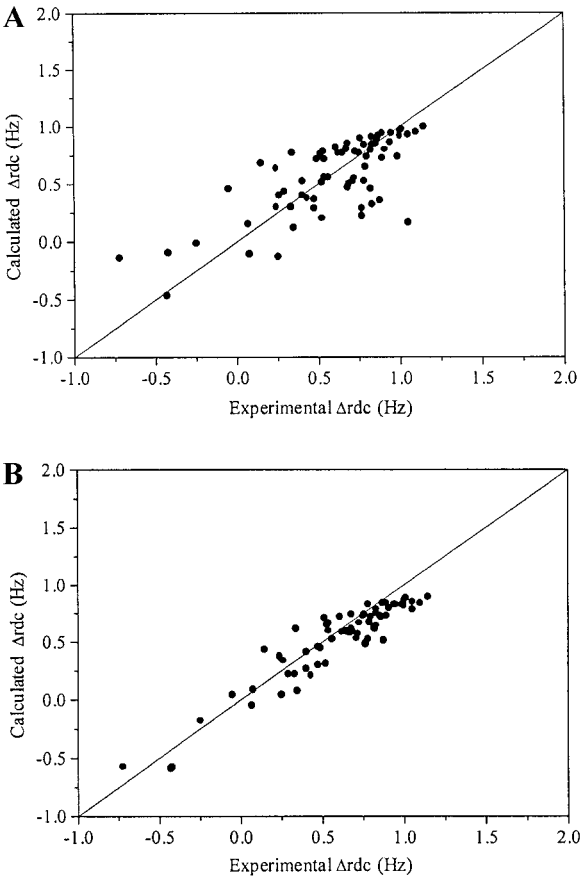

Figure 2. Experimental versus calculated Δrdc values for the oxidized form using the family of conformers of cyt b_{562} calculated without Δrdc (Arnesano et al., 1999) (panel A, r = 0.74) and using the family calculated with the inclusion of Δrdc (panel B, r = 0.93). The solid lines represent the best fit of the points.

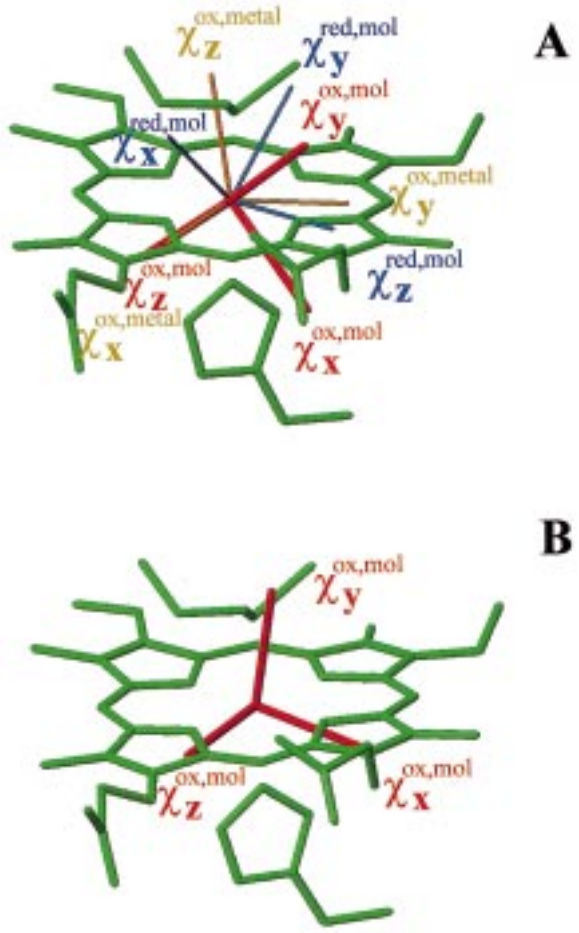

Figure 3. Comparison between calculated (A) and experimental (B) χ_{ox}^{mol} tensors in cyt b_{562}. The axes of the χ_{ox}^{mol} tensor are shown as thick lines colored in red; the axes of the χ_{ox}^{metal} tensor and the χ_{red}^{mol} tensor are shown as thin lines colored in yellow and blue, respectively.

$\Delta\chi^{mol}$ values are needed for the solution structure calculations (see Materials and methods). For the oxidized cyt b_{562} the initial $\Delta\chi^{mol}$ values were $\Delta\chi_{ax}^{mol} = -0.98 \times 10^{-32}$ m^3, $\Delta\chi_{rh}^{mol} = 1.08 \times 10^{-32}$ m^3.

When the Δrdc constraints were used together with all the other constraints in structural calculations from the beginning of simulated annealing, convergence was reached after two cycles of calculations and the program yielded a family of conformers satisfying all the experimental constraints. The output is consistent with the new Δrdc constraints and substantially of the same quality, in terms of RMSD, as for the structures obtained with NOEs, pcs and $^3J_{HNH\alpha}$. The mean deviation between calculated and experimental Δrdc values is much smaller for the families obtained including the new Δrdc constraints than for the initial families obtained without these constraints, indicating that there have been small structural changes which better satisfy the Δrdc constraints. The correlation coefficient r between the calculated and measured Δrdc values is much higher with the inclusion of Δrdc (r = 0.93) than for the family obtained without the rdc constraints (r = 0.74) (Figure 2). However, already after the first structural refinement using these constraints, this correlation has improved significantly.

The final χ^{mol} tensor parameters are reported in Table 1, together with the values relative to the χ^{metal} tensor of the metal ion, obtained from the fitting of pcs. The χ^{metal} tensor parameters were already obtained from pcs (Arnesano et al., 1999). Here, the final χ^{metal} tensor has been recalculated by fitting pcs values to the final family of conformers obtained using rdc.

The backbone RMSD values of the family of conformers of oxidized cyt b_{562} (with NOE, $^3J_{HNH\alpha}$ and pcs constraints) without and with Δrdc constraints are the same within the experimental error (0.42 $\pm$ 0.06 Å and 0.50 $\pm$ 0.10 Å, respectively), whereas the average NOE and van der Waals target function is slightly higher for the latter family (0.76$\pm$ 0.06 Å^2 and 1.15 $\pm$ 0.11 Å^2, respectively). The overall folding of the protein obtained with Δrdc constraints is essentially identical to that obtained without such constraints. The large number of NOE and pcs constraints used in the previous structure calculations reduces the improvement in structure resolution produced by the use of Δrdc but, even in the present example, the new family, which satisfies all sets of constraints, is more accurate than the family obtained without the Δrdc constraints. The family obtained without Δrdc back calculates Δrdc values rather different from the actual ones. This is reflected by the error and by the initial $\Delta\chi^{mol}$ values.

The structure, which has been calculated with all the sets of constraints, despite having an RMSD similar to that previously available, has minimized to a quite satisfactory level the initial disagreements between experimental and calculated constraints, as shown in Table 2, by the negligible increase of the target function. The R-factors (Clore and Garret, 1999) are 0.08 for the family obtained including the new Δrdc constraints and 0.18 for the initial family obtained without these constraints.

The analysis of both structures (with and without Δrdc) through the program PROCHECK (Laskowski et al., 1993, 1996) has shown that the structure refined with Δrdc has a better geometrical quality. Indeed, the family of conformers, calculated without the use of the Δrdc constraints, has 78.0% of the residues in the most favored regions, 19.3% in the allowed regions, 1.8% in the generously allowed regions and 0.9% in the disallowed regions. For the family of conformers, calculated with the inclusion of the Δrdc constraints, these values are 80.1% for the most favored regions, 18.0% for the allowed regions, 1.3% for the generously allowed regions and 0.6% for the disallowed regions. In addition, in the latter case the number of residues belonging to helical structures increases for helices α3 and α4 and there is an extra 3_{10} helix (from residue 45 to 49), reported in the X-ray structure (Hamada et al., 1995) but not detected in the structure family obtained without rdc.

χ^{mol}_{red} tensor of the reduced form

The Δrdc values have also been determined for the reduced form, in order to obtain the χ^{mol}_{red} tensor for this diamagnetic species. The assignment of NMR spectra of the reduced form has been presently completed in our laboratory and deposited in the BioMagResBank. For this form, 47 non-degenerate resonances were assigned at the time of the experiments and for these, ^{1}H-^{15}N ^{1}J couplings have been measured. Their values are available as Supplementary material (Table 2). In deriving the Δrdc values from Equation 2, the same values of δ_{DFS} as for the oxidized form were used. The ^{1}H-^{15}N ^{1}J values (see Figure 1) were corrected by these values and the resulting Δrdc are available as Supplementary material (Table 4).

Because the solution structure of the reduced form is not available, the Δrdc values of the reduced species were not used in structural calculations, but only for obtaining the χ^{mol}_{red} tensor parameters. The Δrdc values were fitted, according to Equation 4, using the structure of the oxidized form. This assumes that only small structural rearrangements occur upon introduction of one electron. The validity of this assumption can be checked through the analysis of the quality of the fitting. Sample calculations have been performed using different sub-sets of data, which all provided the same tensor parameters, within the experimental error. The 47 Δrdc values are enough, in number, to determine the χ^{mol}_{red} tensor parameters which are reported in Table 1.

Comparison of the χ^{mol} tensors of oxidized and reduced cytochrome b_{562} with the χ^{metal} tensor of the metal ion

The magnetic anisotropy of the oxidized paramagnetic molecule, χ^{mol}_{ox}, is the sum of two contributions: that arising from the protein matrix plus the reduced heme, which is the magnetic anisotropy of the diamagnetic state, and that produced by the magnetic anisotropy of the paramagnetic metal ion. The latter has a large magnetic anisotropy arising from spin-orbit coupling and has been already estimated from the pcs (Arnesano et al., 1999).

The sum of the χ^{mol}_{red} tensor obtained from rdc data on the reduced species and the χ^{metal}_{ox} tensor of the metal ion (Arnesano et al., 1999) provides the calculated χ^{mol}_{ox} tensor (see Table 1 and Figure 3), which is in satisfactory agreement with the experimental values, especially if it is considered that the structure of the reduced species is not minimized with Δrdc. The

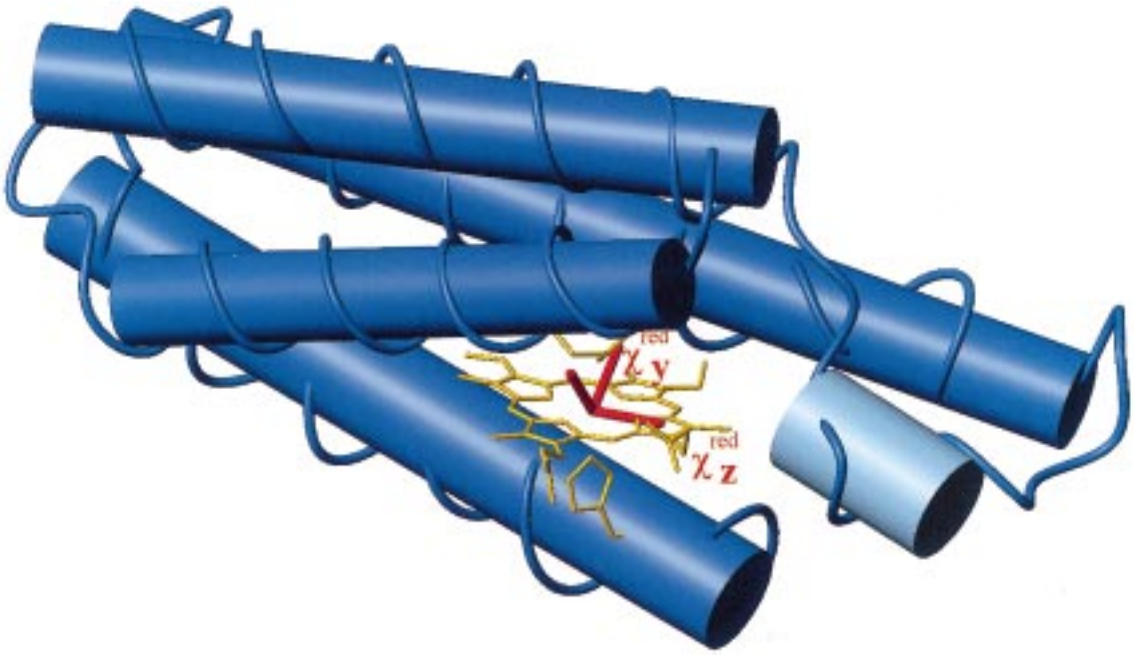

Figure 4. The diamagnetic susceptibility tensor χ_{red}^{mol} in the protein frame. The helical secondary structure elements are shown as cylinders: the α helices in blue and the 3_{10} helix in light blue.

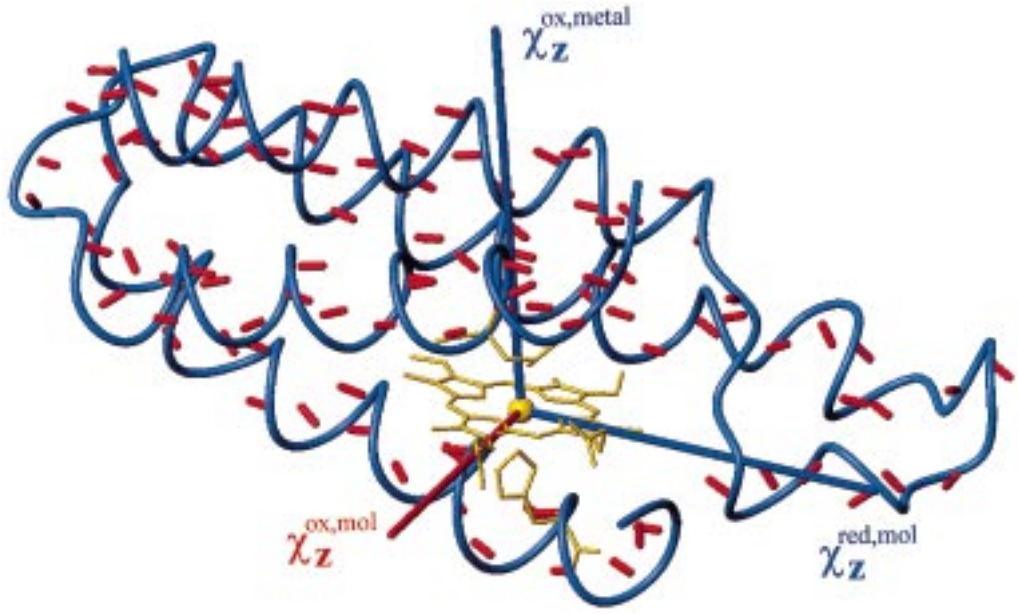

Figure 5. The z axis directions of the tensors χ_{ox}^{mol} (colored in red), χ_{red}^{mol} and χ_{ox}^{metal} (colored in blue) of cyt b_{562}, shown in the protein frame. The directions of the NH bonds are also depicted with a thick red line.

above conclusion gives us confidence for the further analysis of the magnetic properties of the system.

In the reduced diamagnetic state of the protein, partial orientation derives from the magnetic susceptibility anisotropy due to peptide bonds (Tigelaar and Flygare, 1972; Williamson and Asakura, 1993), aromatic side chains (Giessner-Prettre and Pullman, 1987) and the heme moiety (Bothner-By et al., 1985). The contribution of the aromatic side chains is small (Giessner-Prettre and Pullman, 1987) and, as all the aromatic rings in this protein flip rapidly in solution and therefore span multiple conformations, their contribution partially averages out. Therefore, it is neglected in this analysis. The $\Delta\chi_{ax}$ value for the heme contribution is about -1.3×10^{-32} m^3 (Bothner-By et al., 1985). It should be noted that the axial anisotropy is negative, i.e., the component of the tensor perpendicular to the heme plane is smaller than those in the heme plane. The magnetic anisotropy of each peptide group is axially symmetric and is oriented perpendicular to the peptide plane, and with a magnetic anisotropy $\Delta\chi_{ax} = -2\times10^{-34}$ m^3 (Tigelaar and Flygare, 1972; Williamson and Asakura, 1993). Their contribution can be estimated from the structure of the molecule. Considering that in a helical structure the peptide planes are roughly parallel to the helix axis direction, the diamagnetic susceptibility anisotropies for each peptide bond sum up in this direction. As a consequence, the helix has the z axis of the magnetic susceptibility along its direction and therefore tends to orient parallel to the magnetic field, as experimentally found. The contribution of the four-helix bundle to the magnetic anisotropy is the tensorial sum of the contributions of each helix. By summing the $\Delta\chi$ contribution of each peptide bond and by taking into account their orientation in the protein frame, a contribution of 0.7×10^{-32} m^3 is obtained. The tensorial sum of the contribution of all peptide bonds and of the heme provides an axial anisotropy $\Delta\chi_{ax} = 1.4 \times 10^{-32}$ m^3 and a rhombic anisotropy $\Delta\chi_{rh} = -1.2 \times 10^{-32}$ m^3. Taking into account the simplicity of the model, the agreement with the experimental values can be considered quite satisfactory. The z axis of the magnetic susceptibility tensor is coincident, within 10°, with the experimental one. A larger error (30°) is found for the rhombic axes. Figure 4 shows the orientation of the experimental diamagnetic susceptibility anisotropy tensor in the protein frame with the z axis almost coincident with the four-helix bundle axis and parallel to a vector connecting the β and δ heme pyrrole nitrogens.

The z axis of the magnetic susceptibility tensor of the paramagnetic metal ion, χ_{ox}^{metal}, is perpendicular to the heme plane and, therefore, is almost orthogonal to the z axis of the diamagnetic susceptibility tensor, χ_{red}^{mol} (see Table 1). The resulting molecular magnetic anisotropy tensor χ_{ox}^{mol} has, therefore, the z axis perpendicular to the above two directions and a negative $\Delta\chi_{ax}$ value. Thus, in a magnetic field the molecule is preferentially oriented orthogonal to the z axis, which is shown in red in Figure 5.

The above analysis indicates that the magnitude and the directions of the resulting χ_{ox}^{mol} tensor of the oxidized form are determined by both the diamagnetic and the metal ion contributions to magnetic susceptibility anisotropy. Therefore, the four-helix bundle folding plays a large effect in the magnetic orientation of cyt b_{562} and probably of proteins characterized by the same folding motif. This effect is comparable with that of a paramagnetic metal ion. This is at variance to what has been observed for oxidized cyt b_5 (Banci et al., 1998), which also contains a *b*-type heme with a low spin iron (III) and which has an almost spherical shape. In this case the orientation of the molecule induced by the magnetic field was essentially dominated by the paramagnetic contribution, the diamagnetic one being very small.

Conclusions

In this research it has been shown that the use of Δrdc of the ^{1}H-^{15}N dipole in cyt b_{562} as structural constraints since the early steps of calculations, through a general equation, represents a reliable general strategy. The resulting structure is only slightly different compared to that previously obtained with NOEs, $^3J_{HNH\alpha}$ values and pcs. However, the use of Δrdc has allowed the determination of a more accurate structure and of higher quality in terms of the Ramachandran plot. The whole approach has allowed to separate the various contributions to the overall molecular magnetic anisotropy, $\Delta\chi^{mol}$.

The four-helix bundle folding by itself causes a relatively large molecular orientation in high magnetic fields and therefore is suitable for the exploitation of rdc in structural calculations and refinement.

Acknowledgements

This work was supported by the European Community (TMR-LSF Contract ERBFMGECT950033,

TMR contract FMRX-CT98-0230), by Italian CNR (Progetto Finalizzato Biotecnologie 99.00509.PF49) and by MURST ex 40%.

The authors thank Prof. Alan R. Fersht and Dr. Paul D. Barker for providing the ^{15}N-labelled protein sample, Mr. Michael Assfalg for providing the ^{15}N and ^{1}H chemical shifts of reduced cytochrome b_{562} and Dr. Antonio Rosato for helpful discussions. F.A. gratefully acknowledges financial support for visiting the SON NMR Large Scale Facility in Utrecht.

Supplementary material

The following supporting information is available from the corresponding authors: experimental J values at 18.7 and 11.7 T magnetic field for oxidized (Table 1) and reduced (Table 2) cytochrome b_{562} and the root mean square differences between the two sets of experiments, as well as the experimental Δrdc values for both the oxidized (Table 3) and the reduced (Table 4) form of cytochrome b_{562}.

References

Arnesano, F., Banci, L., Bertini, I., Faraone-Mennella, J., Rosato, A., Barker, P.D. and Fersht, A.R. (1999) *Biochemistry*, **38**, 8657–8670.

Arnesano, F., Banci, L., Bertini, I. and Felli, I.C. (1998) *Biochemistry*, **37**, 173–184.

Banci, L., Bertini, I., Gray, H.B., Luchinat, C., Reddig, T., Rosato, A. and Turano, P. (1997) *Biochemistry*, **36**, 9867–9877.

Banci, L., Bertini, I., Huber, J.G., Luchinat, C. and Rosato, A. (1998) *J. Am. Chem. Soc.*, **120**, 12903–12909.

Bayer, P., Varani, L. and Varani, G. (1999) *J. Biomol. NMR*, **14**, 149–155.

Bentrop, D., Bertini, I., Cremonini, M.A., Forsén, S., Luchinat, C. and Malmendal, A. (1997) *Biochemistry*, **36**, 11605–11618.

Bertini, I., Luchinat, C. and Rosato, A. (1996) *Prog. Biophys. Mol. Biol.*, **66**, 43–80.

Biekofsky, R.R., Muskett, F.W., Schmidt, J.M., Martin, S.R., Browne, J.P., Bayley, P.M. and Feeney, J. (1999) *FEBS Lett.*, **460**, 519–526.

Bolon, P.J., Al-Hashimi, H.M. and Prestegard, J.H. (1999) *J. Mol. Biol.*, **293**, 107–115.

Bothner-By, A.A. (1996) In *Encyclopedia of Nuclear Magnetic Resonance* (Eds., Grant, D.M. and Harris, R.K.), John Wiley and Sons, Chichester, pp. 2932–2938.

Bothner-By, A.A., Domaille, J.P. and Gayathri, C. (1981) *J. Am. Chem. Soc.*, **103**, 5602–5603.

Bothner-By, A.A., Gayathri, C., van Zijl, P.C.M. and Maclean, C. (1984) *J. Magn. Reson.*, **56**, 456–462.

Bothner-By, A.A., Gayathri, C., van Zijl, P.C.M., Maclean, C., Lai, J.-J. and Smith, K.M. (1985) *Magn. Reson. Chem.*, **23**, 935–938.

Clore, G.M. and Garret, D.S. (1999) *J. Am. Chem. Soc.*, **121**, 9008–9012.

Clore, G.M. and Gronenborn, A.M. (1998) *Proc. Natl. Acad. Sci. USA*, **95**, 5891–5898.

Clore, G.M., Gronenborn, A.M. and Tjandra, N. (1998) *J. Magn. Reson.*, **131**, 159–162.

Domaille, J.P. (1980) *J. Am. Chem. Soc.*, **102**, 5392–5393.

Fischer, M.W., Losonczi, J.A., Weaver, J.L. and Prestegard, J.H. (1999) *Biochemistry*, **38**, 9013–9022.

Gayathri, C., Bothner-By, A.A., van Zijl, P.C.M. and Maclean, C. (1982) *Chem. Phys. Lett.*, **87**, 192–196.

Giessner-Prettre, C. and Pullman, B. (1987) *Q. Rev. Biophys.*, **20**, 113–172.

Hamada, K., Bethge, P.H. and Mathews, F.S. (1995) *J. Mol. Biol.*, **247**, 947–962.

Hiyama, Y., Niu, C.H., Silverston, J.V., Bavoso, A. and Torchia, D.A. (1988) *J. Am. Chem. Soc.*, **110**, 2378–2383.

Johnson, B.A. and Blevins, R.A. (1994) *J. Biomol. NMR*, **4**, 603–614.

Laskowski, R.A., MacArthur, M.W., Moss, D.S. and Thornton, J.M. (1993) *J. Appl. Crystallogr.*, **26**, 283–291.

Laskowski, R.A., Rullmann, J.A.C., MacArthur, M.W., Kaptein, R. and Thornton, J.M. (1996) *J. Biomol. NMR*, **8**, 477–486.

Lohman, J.A.B. and Maclean, C. (1978a) *Chem. Phys.*, **35**, 269–274.

Lohman, J.A.B. and Maclean, C. (1978b) *Chem. Phys. Lett.*, **58**, 483–486.

Lohman, J.A.B. and Maclean, C. (1981) *J. Magn. Reson.*, **42**, 5–13.

Tigelaar, H.L. and Flygare, W.H. (1972) *J. Am. Chem. Soc.*, **94**, 343–346.

Tjandra, N., Feller, S.E., Pastor, R.W. and Bax, A. (1995) *J. Am. Chem. Soc.*, **117**, 12562–12566.

Tjandra, N., Grzesiek, S. and Bax, A. (1996) *J. Am. Chem. Soc.*, **118**, 6264–6272.

Tjandra, N., Omichinski, J.G., Gronenborn, A.M., Clore, G.M. and Bax, A. (1997) *Nat. Struct. Biol.*, **4**, 732–738.

Tolman, J.R., Flanagan, J.M., Kennedy, M.A. and Prestegard, J.H. (1995) *Proc. Natl. Acad. Sci. USA*, **92**, 9279–9283.

Tolman, J.R. and Prestegard, J.H. (1996) *J. Magn. Reson.*, **B112**, 245–252.

van Zijl, P.C.M., Ruessink, B.H., Bulthuis, J. and Maclean, C. (1984) *Acc. Chem. Res.*, **17**, 172–180.

Werbelow, L. (1996) In *Encyclopedia of Nuclear Magnetic Resonance* (Eds., Grant, D.M. and Harris, R.K.), John Wiley & Sons, Chichester, pp. 1776–1783.

Williamson, M.P. and Asakura, T. (1993) *J. Magn. Reson.*, **B101**, 63–71.

Wu, J.Z., La Mar, G.N., Yu, L.P., Lee, K.B., Walker, F.A., Chiu, M.L. and Sligar, S.G. (1991) *Biochemistry*, **30**, 2156–2165.